

Effect of FBG Fiber Dosimeter Division in Sensing Capability for Low Radiation Doses

Taghreed Khalid Hameed⁽¹⁾

taghreedkhalid@uomustansiriyah.edu.iq

Wasmaa A. Jabbar⁽²⁾

wasmaajabbar@uomustansiriyah.edu.iq

Zina Al_dagistany⁽³⁾

kkzlls1234@gmail.com

AyserA. Hemed⁽⁴⁾

ayser.hemed@uomustansiriyah.edu.iq

Sami Salman Chiad⁽⁵⁾

dr.sami@uomustansiriyah.edu.iq

Department of Physics, College of Education, Mustansiriyah University,
Baghdad-Iraq

Abstract:

A fiber Bragg grating (FBG) as a dosimeter is developed in this simulation study (based on Optisystem 21 software) by dividing its region into five individual regions. The division includes the same properties for all regions, which is a standard SiO₂ optical fiber material. In dosimeters, it is convenient to introduce dopants to increase the fiber sensitivity. The new design accepts dopants and can work without such a dopant. Measurements for sensing deflected signals from the FBG sensor confirmed increased sensitivity for low-rate radiation doses in comparison to one bulk region in a traditional fiber dosimeter. The sensitivity of this dosimeter is based on both the FWHM line shape function and the amplitude of the deflected signals. The FBG dosimeter sensor can respond to low-dose radiation in a noticeable manner according to the type of applied simulated effect. Dosimeter body division for multi-regions gives rise to sensitivity in comparison to the traditional bulk region. The measured FWHM from the line-shape function for overall observed signals fluctuates from 0.374 MHz under applied temperature, stress x, y, z, and strain to 0.358, 0.373, 0.3733, 0.368, and 0.3737 MHz,

respectively. While this range follows different fitting functions: Sin, Exp.Decay, SinSqu., Exp.Decay3, and GaussAmpl. For last effects, according to measured effect. The same measurements were carried out for signal amplitude variation, with these effects giving a variety of relationships indicating their existing contribution. Results confirmed an efficient tool for use in sensing for low x-ray and gamma ray radiation dose applications versus traditional bulk FBG sensor type.

Keywords: Dosimeter, Fiber Bragg Grating, x-ray, Gamma ray, line width Function, Deflection.

I. Results and disscussion

Introduction:

Due to advantages of fiber Bragg gratings (FBGs) over other technologies, the optical systems' capacity is greatly increased by wavelength division multiplexer (WDM). The chemical makeup and photosensitization technique utilized in the creation of FBGs have a significant impact on their radiation sensitivity [1]. For fibers without hydrogen loading, the shape and amplitude of the grating spectra did not change throughout the course of the lengthy radiation period; however, for fibers with hydrogen loading, there were only minor alterations [2, 3]. They have proven to be very promising for a variety of sensing applications where quasi-distributed (QD) measurements for significant physical quantities are needed. In additional to conventional benefits to optical fibers, reported in Ref. [4], Practical QD sensing can be achieved through their multiplexing via comparable methods that have been used with fiber-optic sensors, such as WDM, spatial-division-multiplexing, time-division-multiplexing, and their combinations [4].

The technique of single-pulse FBG manufacture with an excimer laser system and an interferometric inscription scheme was demonstrated in Ref. [5]. This research resulted in the development of a method for creating arrays of these diffraction structures while drawing an optical cable. The optical fibers' strength characteristics are maintained when employing this technique.

Nowadays, monitoring of ionizing radiations (IRs) is very important in different fields. In particular, a quantitative detection of IRs is crucial in environmental, industrial and health applications. In radiotherapy, the main objective is the measurement of the "dose", i.e., the absorbed energy per unit of mass that is delivered to the patient [6]. Optical fiber sensors (OFS) can in principle match all these features. OFS, based on telecommunication technology, have been successfully used for temperature, strain, pressure and

acceleration monitoring in many different areas of research. They have been recently proven also as powerful tools for IR monitoring [6, 7, 8, 9].

Space, nuclear power plants, storage facilities for radioactive waste, reactor disassembly sites, and high-energy physics facilities are a few examples of hostile settings [10]. Different temperature ranges and irradiation circumstances, such as particle type, fluence (dosage), and flux (dose rate), are characteristics of each of them. (The amount of energy deposited into the material of interest, in this case silica, is known as the dosage. $\text{SiO}_2 = 1 \text{ Gy} = 1 \text{ J/kg}$. The energy's deposition speed, measured in Gy/s, is the dosage rate. The rad, which is an older dosage unit ($1 \text{ Gy} = 100 \text{ rad}$), is utilized in several articles. Space, for instance, is characterized by high temperature changes (between $-200 \text{ }^\circ\text{C}$ and $300 \text{ }^\circ\text{C}$) but low exposure rates and dosages (less than $10\text{--}3 \text{ Gy/h}$ and 10 kGy , respectively). Conversely, fusion-focused facilities operate at room temperature and are characterized by very high dose rates (up to MGy/s) and low doses (less than 1 kGy), while the nuclear reactor core is linked to very high radiation rates (up to GGy) and high temperatures (up to $800 \text{ }^\circ\text{C}$) [11].

In addition to optical communications [12], laser pulse alterations associated phenomena [13, 14], and on board sensors, such as in nuclear and smart space propulsion systems, FBGs have also been investigated for space fiber optic communication systems [15].

Coating layers outside of optical fibers can potentially be impacted by radiation. Numerous investigations conducted by Rizzolo and coworkers have demonstrated that temperature and radiation exposure can alter the elastic characteristics of certain coating types or the coating-fiber interface. These modifications may affect the appropriate calibration of distributed temperature measurements made using optical frequency domain reflectometry (OFDR) [16].

When a material—like a semiconductor or dielectric—is subjected to intense radiation, a series of reactions may occur. The following related phenomena are related to photon energy in the case of uncharged radiation (photons of X and Gamma); these are organized from lower to higher energies, respectively: pair creation, photoelectric effect, Compton scattering, and Rayleigh scattering. There are two stages in the interaction between neutrons and γ -rays with matter. The material absorbs the incident particle's kinetic energy in two ways: first, as the charged particles slow down, the energy is deposited in the material. Eventually, this resulted in an alteration

to the atomic and electronic structure. This in turn alters the properties of the material and, consequently, the features of the devices made from these materials [15].

The fiber's optical attenuation can rise noticeably even at low cumulative dosages. The creation of so-called color centers, or the trapping of radiolytic electrons and holes at fiber silica defect sites, is the main cause of radiation-induced attenuation (RIA). When optical wavelengths are higher, the resultant attenuation decreases. In fact, color centers mostly absorb in the visible and ultraviolet regions of the spectrum, with infrared absorption tails.

The primary component of optical fibers now in use is silicon dioxide (SiO₂), sometimes referred to as pure glass. Although they have limits, glass made of fluoride and plastic fibers are also in use. Particularly plastic optical fibers exhibit higher attenuation than glass fibers, which renders them less appropriate for optical sensing in radiation-prone situations. Defect centers may arise in the silica substance of optical fibers when exposed to radiation.

The primary reason responsible for attenuation loss is defect centers, also known as color centers. The optical fiber's refractive index changes as a result of radiation exposure because the fiber matrix structure is damaged, which raises the fiber absorption loss. The transmitted signal absorbs more energy as a result of the faults creating new energy levels inside the band gap. Radiation Induced Attenuation (RIA) is the term used to describe the increase in absorption [17].

Both the development of new color centers and their recovery compete during irradiation. As a result, the dose-rate also affects how much attenuation is induced. The parameters pertaining to radiation include particle types (such as x-ray, γ -ray, protons, and neutrons), temperature, dose (fluence), dose-rate (flush), and application purpose (such as data transfer sensing or diagnostics). The characteristics of the fiber include its composition (core and cladding), manufacturing process (stoichiometry, drawing parameters), opto-geometric parameters, coating type, and light-guiding properties. The RIA can be computed using the Lambert-Beer law definition [18]:

$$\alpha_{RIA} \left(\frac{dB}{m} \right) = \frac{10}{L(m)} \cdot \log \frac{I}{I_0} \quad (3)$$

where I and I_0 represent the transmitted signal intensities, respectively, at a specific moment and prior to the start of irradiation.

Studies have demonstrated that gamma irradiation in nuclear settings weakens fibers because it alters the refractive index. This is reliant on the chemical makeup and photosensitization method employed in the fiber composition. Radiation-Produced When subjected to gamma radiation, the Ge atoms in the optical fiber core are excited, which is the primary source of attenuation RIA. Because of total internal reflection, which results from the difference in the index of refraction between the fiber's cladding and core, light is guided through the core of the optical fibers.

Germanium is a dopant that is used to improve light-guiding qualities by raising the index of refraction between the cladding and core. Attenuation is the result of absorption and scattering, which causes the power of light moving through the optical fiber to decrease with distance. The definition is given in dB/km, or decibels per kilometer. However, due to their small spectrum range of less than 5 nm or narrow wavelength encoding, FBGs appear to be immune to the optical power loss caused by broadband radiation [17].

As demonstrated in Figures 1 and 2 [19], gamma irradiation of Ge-doped fibers causes a shift in the effective refractive index, which in turn causes a radiation-induced Bragg wavelength (BW) shift.

The photosensitive fiber's RIA lowers the baseline in Figure 1, but there is no attenuation in Figure 2 [20]. The peak position's induced BW shift indicates that FBGs could be employed for dosimetry [17].

The silica fiber doped with germanium exhibits significant photosensitivity. The photosensitivity of the fiber can be further increased with the addition of hydrogen loading and boron co-doping. The combination of hydrogen loading and germanium doping makes the fiber more radiation sensitive [10].

At a wavelength of 1550 nm, Silicate and Germano-silicate glass exhibit attenuation rates as low as 0.20 dB/km. Germanium is a dopant that is used to improve light-guiding qualities by raising the indices of refraction between the cladding and core [21]. The silica fiber doped with germanium exhibits significant photosensitivity. Additional hydrogen loading and boron co-doping can further increase the fiber's photosensitivity [22].

The sensitivity of FBGs written in Ge-doped and hydrogen-loaded fibers to gamma irradiation was higher than that of those without hydrogen loading when exposed to high doses of gamma radiation [23].

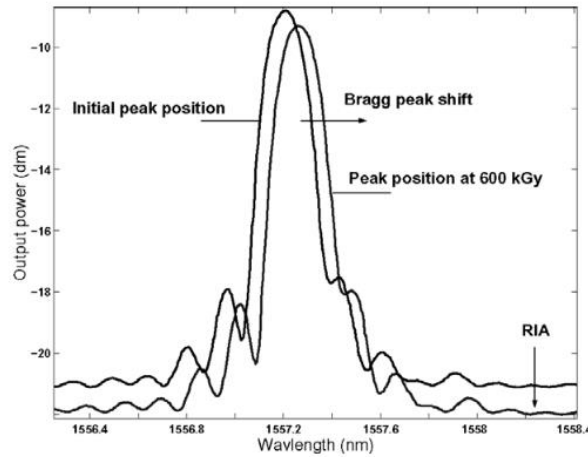


Figure 1. Bragg peak shift caused by radiation, with RIA lowering the baseline [19].

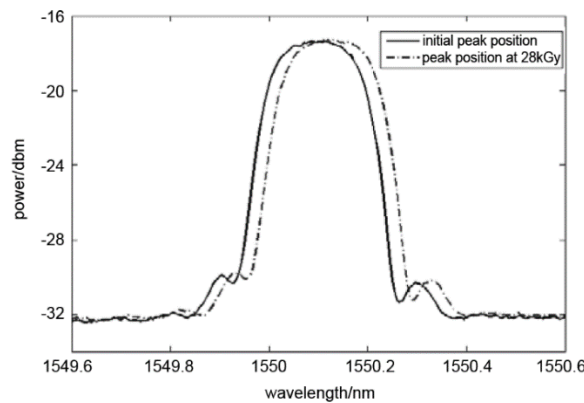


Figure 2. Bragg peak shift caused by radiation, without RIA [20].

In the literature, a number of RIA growth and recovery models have been put out. A straightforward power-law model has been explored a few times in the literature as a potential explanation for the induced absorption growth [15]:

$$RIA = \alpha D^\beta \quad (1)$$

where α and β are empirical constants and D is the total dosage.

Following the equation, n -th order kinetics has been used to characterize the recovery following irradiation [15]:

$$RIA = (RIA_o - RIA_f)(1 + ct)^{\frac{-1}{(n-1)}} + RIA_f \quad (2)$$

where $c \equiv \frac{1}{\tau}(2^{n-1} - 1)$, RIA_o and RIA_f are the initial and final values respectively of the induced attenuation, τ is the half-height lifetime of the

recovery and n is the material-dependent kinetic order. The creation of color centers in silica fibers caused by radiation has also been studied using fractal kinetics.

I. Theory of FBG based Radiation Sensing

When fiber is exposed to radiation, it is anticipated that RIA, radiation-induced emission (RIE), and radiation-induced compaction (RIC) will manifest. Within this setting, ionizing radiation-induced defects alter the effective refractive index of gratings, changing the BW, or $\lambda_B(T) \rightarrow \lambda_B(d, T)$, where d represents the total radiation dosage. The degree to which $\lambda_B(T)$ and K_T , where K_T is the temperature sensitivity coefficient, are radiation-sensitive determines whether or not FBGs may be used for temperature sensing in radiation conditions [24]. The shift of BW as a function of radiation and temperature is given by taking into account the simultaneous effects of radiation and temperature on FBGs [24];

$$\lambda_B(d, T) = 2n(d, T)\Lambda(d, T)$$

Only terms up to the second order in the radiation-induced wavelength shift are kept when the Taylor series expansion is carried out, ignoring temperature-dependent high order terms. This allows one to derive [24];

$$\Delta\lambda_B(d, T) = 2n \left[\Lambda \frac{\partial n}{\partial d} + n \frac{\partial \Lambda}{\partial d} \right]_{d=d_0, T=T_0} \Delta d + 2 \left[\Lambda \frac{\partial^2 n}{\partial d^2} + n \frac{\partial^2 \Lambda}{\partial d^2} \right] (\Delta d)^2 + 2 \left[\Lambda \frac{\partial n}{\partial T} + n \frac{\partial \Lambda}{\partial T} \right]_{d=d_0, T=T_0} \Delta T$$

The BW shift caused by temperature variation is the third term in the last calculation, while the first two terms are wavelength shifts caused by radiation. Noting that Ref. [25] is reported alternative calibration for the effect of temperature in FBG sensor.

The objective of the current work is to diagnose and theoretically characterize the FBG response to the applied irradiation rates. Strain, temperature, and stress are all included in this reaction.

II. Simulation set-up

Configuration set-up is given in Fig. 3. According to Ref. [24], there is no effective dependency of fiber dopants on temperature sensitivity during the radiation environment applied to the FBG. Thus, dopantes is ignored for the current FBG material. The study is simulating the expected attenuation and FWHM for the observed reflection spectra.

The design is based on configuring a simple set-up that includes multiple consecutive FBG regions in order to observe each effect separately. Then another part of the reflected signal portion is combined to observe all expected developments for the signal. The FBG parameters in all suggested FBG regions are chosen such that they all have the same parameter values; the only parameter in each region that is subject to variation is the temperature (T), stress-x (MPa), stress-y (MPa), stress-z (MPa), strain (dimensionless) for regions I, II, III, IV, and V, respectively. Each region has 10 mm of length. The FBG type is an ordinary standard uniform index modulation. Due to limitations in Optisystem software, when a parameter is selected as dynamical, instead of a single region, the current five regions are the alternative option. This gives the facility to operate each region-selected effect independently to follow the exact scenario for the fiber region response to irradiation.

Selection for the operational wavelength is based on sensitivity enhancement to the FBG subjects to gamma radiation that exhibits no saturation till 100KGy, as reported in Refs. [26, 17].

The selected light source is a Gaussian pulse generator to exclude any unwanted distortion in the virtual sent signal. To operate the source, a bit sequence-type pulse generator is required via modulation. Another software requirement is the optical delay device for the back-reflected portion of the signal from the FBG. The remaining parts of the set-up are the observations via interrogator for only reflected signals to give the responded signal to the applied effect. For comparison, a WDM combiner is connected from all last reflected signals from the FBG regions this is to observe the WDM overall expected signal.

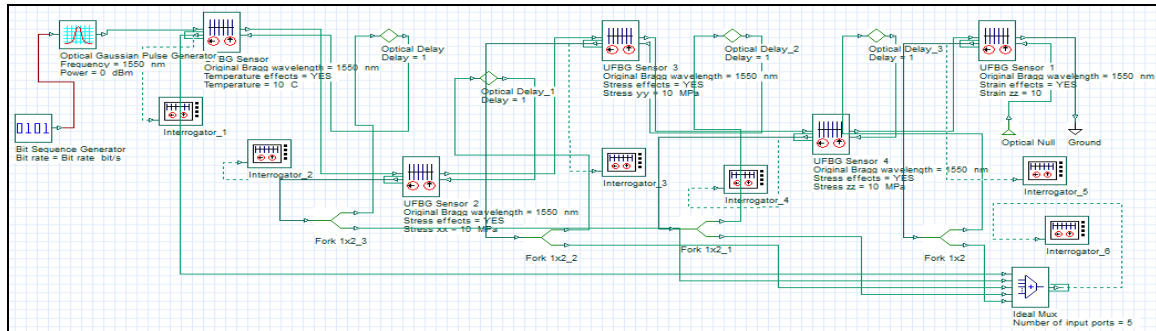


Figure 3. Configuration set-up for a five regions FBG sensor dosimeter. Observations are based on interrogators 1 to 6 from reflected signal by each FBG region.

The dosimeter configuration set-up is situated roughly as reported by Ref. [17]. The applied field is applied longitudinally along multiple sensing zones thanks to the sensors' alignment. There are precisely five sensors in these areas, and their constant BW is 1550 nm. It is believed that radiation impacts affect these sensors independently, meaning that there is a sensor for every effect. Changing a single effect parameter for each sensor throughout each run is the basis for the external effect given to those virtual sensors. Using interrogator visualizer observation, each sensor's reaction is tracked individually. It should be noted that the applied effect value range is intentionally set higher than its actual range in order to amplify the sensor response. The temperature range is 0 to 50 °C. Lastly, the strain effect is altered in only the x direction from 0 to 50. Stress is varied in all x, y, and z directions. All these parameters that supported in the study is summarized in table 1.

Table 1. Parameters applied to individual FBG dosimeter regions to simulate low virtual irradiation doses.

FBG1 Temperature	FBG2 Stress- x	FBG3 Stress- y	FBG4 Stress- z	FBG5 Strain
10	10	10	10	10
20				
30				
40				
50				
10	10	10	10	10
	20			

	30		
	40		
	50		
10	10	10	
	20		
	30		
	40		
	50		
10	10	10	
	20		
	30		
	40		
	50		
10	10		
	20		
	30		
	40		
	50		

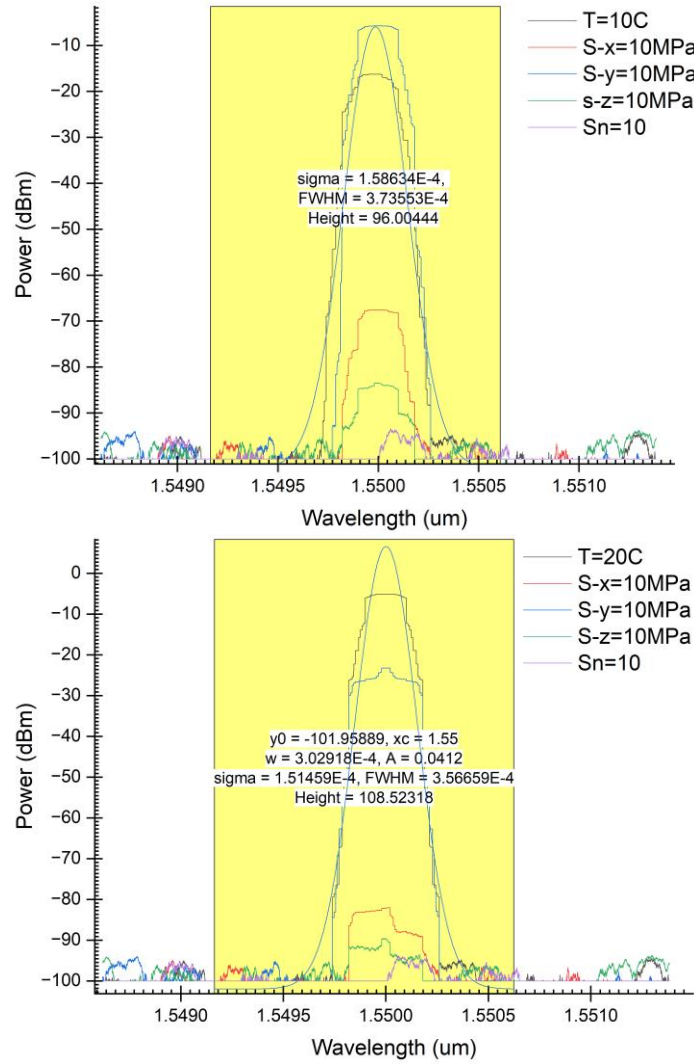
When the FBG is exposed to gamma radiation the saturation of the radiation induced Bragg peak shift occurs towards the longer wavelengths [27]. In comparison between high Ge-content and Hydrogen loaded have produced a BW shift of 160 pm versus 50 pm for undoped fiber both after exposure to dose rate 100 kGy [28, 29]. Ref. [30] and Ref. [31] presented the radiation dose varies (at room temperature) for X and γ rays from $< 1 \text{ Gy/S}$ in medicine to $> \text{MGy/S}$ in Fusion-devoted facilities.

In the following, regions and results for the applied effect will be tracked in a sequence as they appeared in Fig. 3.

1. Effect of applied Temperature on dosimeter signal

Applied temperature on the first FBG region is changed from 10 to 50 °C. During this period, all remaining regions parameters is kept constant. Observation is received from interrogator number 1 in fig. 3. Results are shown in Fig. 4, part A to D, for the tested temperature values, while Fig. 5 gives the WDM overall resulted signal after considering the reflected parts from the five regions. The applied temperature on the first FBG region is

calibrating continues irradiation. Remaining effects is considered temporary constant equal to the value 10.



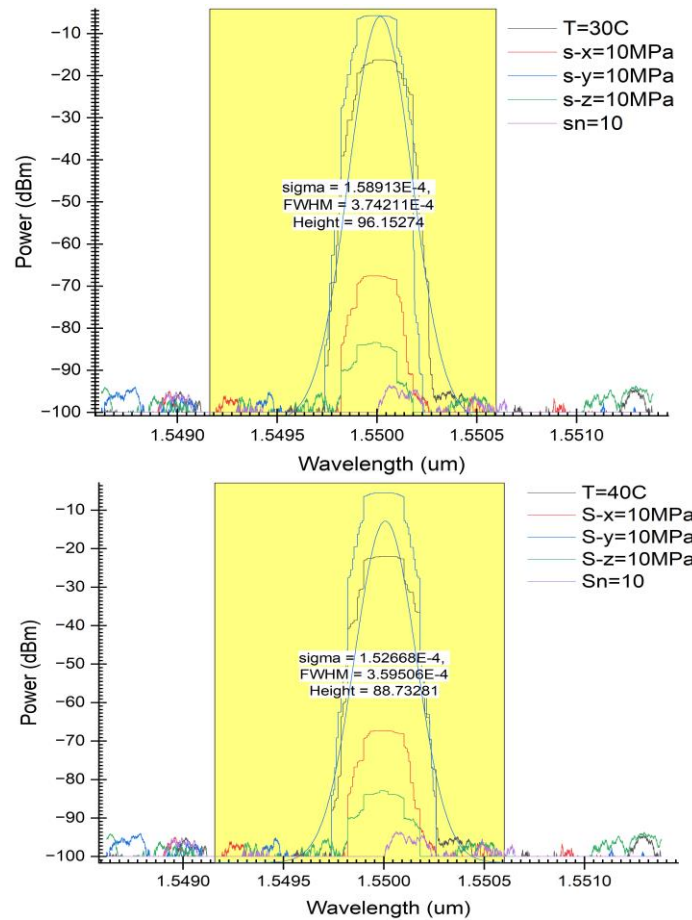


Fig. 4. Individual observations for FBG dosimeter regions response to the applied temperature. Parameters are given inside each shape.

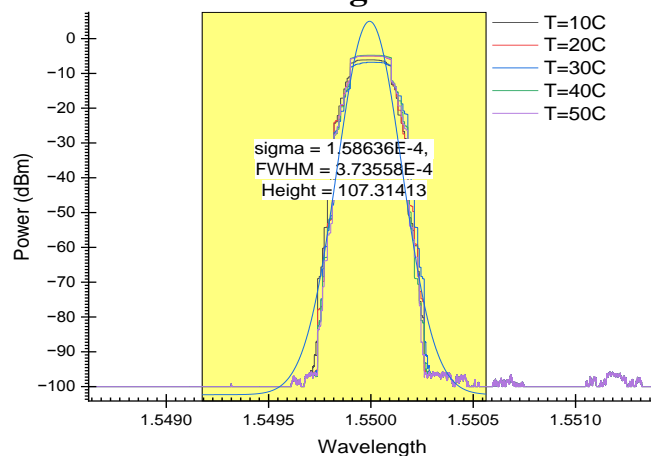


Fig. 5. Multiplexed input WDM for all individual FBG regions reflected signals as a response for temperature variation from 10 to 50 °C.

According to results shown in Fig. 4, the FWHM is changed from $3.56659E-4$ to $3.59506E-4$ nm while the height is changed from 96.00444 to 88.73281 dBm. Both measured from 10 to 50 °C, respectively. The relation between applied T and measured FWHM is follows a sine wave fitting, as shown in Fig. 6.

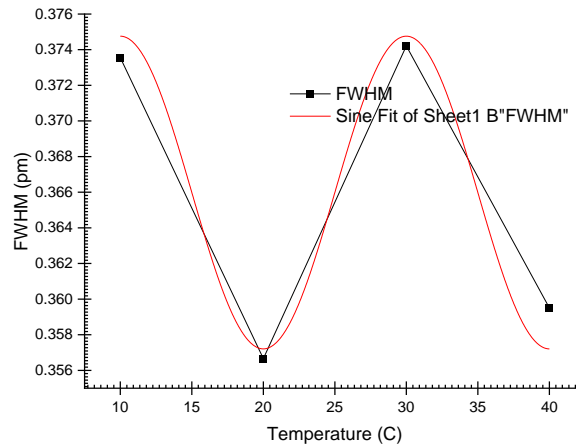


Figure 6. Final relation between applied T and measured reflected signal FWHM from the dosimeter.

While the relation between reflected signal amplitude and applied T is followed a Lorentz function fitting, as shown in Fig. 7.

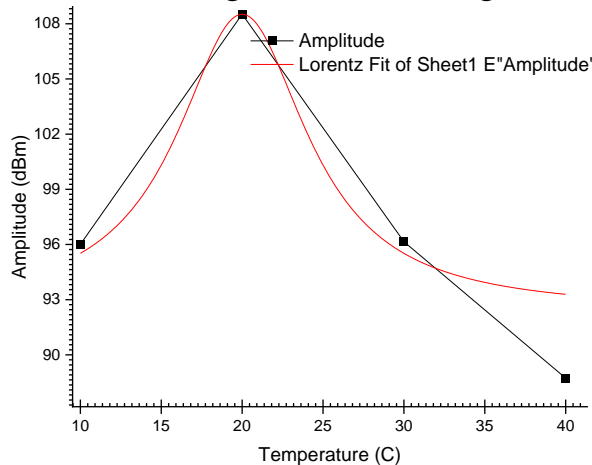
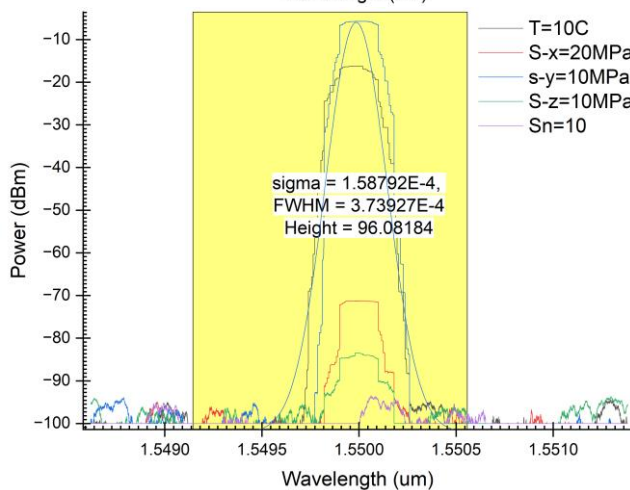
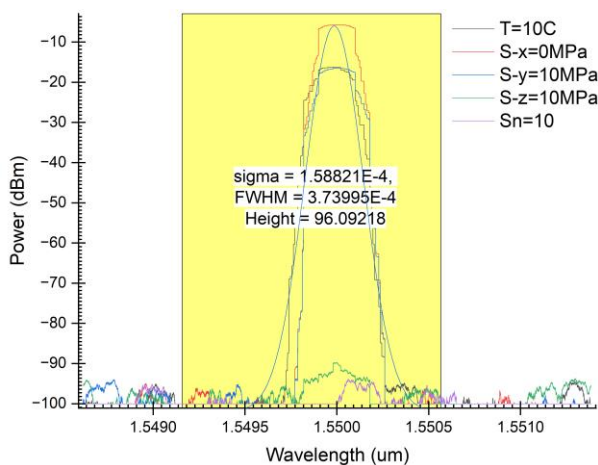


Fig. 7. Final relation between applied T and measured reflected signal amplitude from the dosimeter.

2. Effect of applied Stress x on dosimeter signal

The stress value included as an external effect of radiation is changed from 0 to 50 Mpa for region two of the FBG system. Results are shown in Fig. 8 (individual measurements) and 9 for WDM overall measurement.



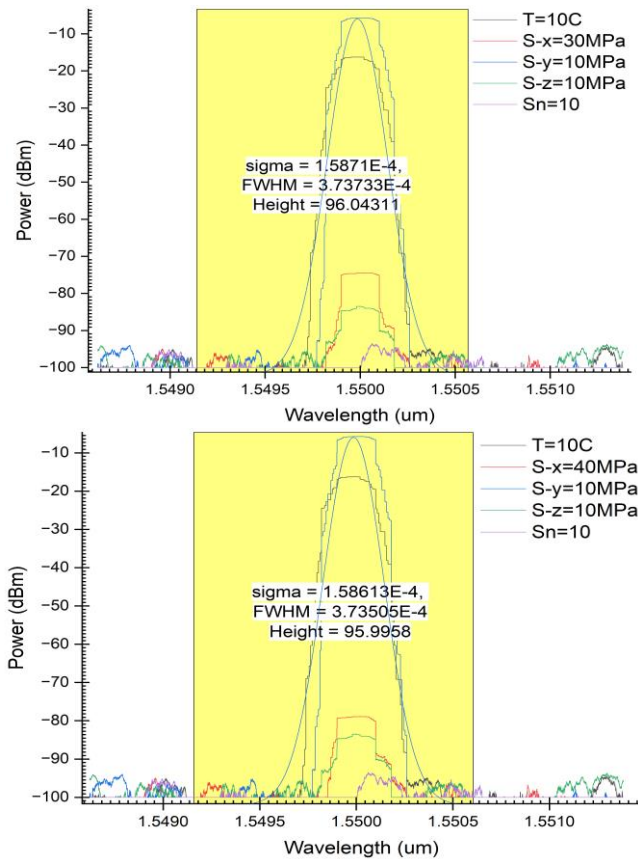


Fig. 8. Individual response for FBG dosimeter regions for stress and strain with applied stress x. Parameters are given inside each shape corresponding the stress variation.

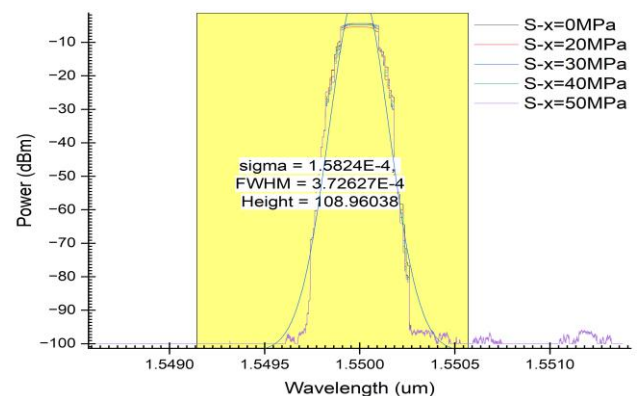


Fig. 9. Multiplexed input WDM for all individual FBG regions reflected signals as a response for stress-x variation from 0 to 50MPa.

Statistics for relations between applied stress-x and FWHM and amplitude for the reflected signal from the FBG dosimeter are given in Fig. 10 and Fig. 11, respectively.

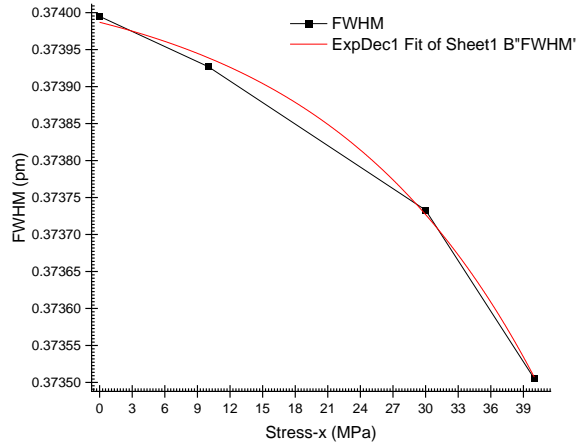


Fig. 10. Final relation between applied stress-x and reflected signal FWHM from the dosimeter.

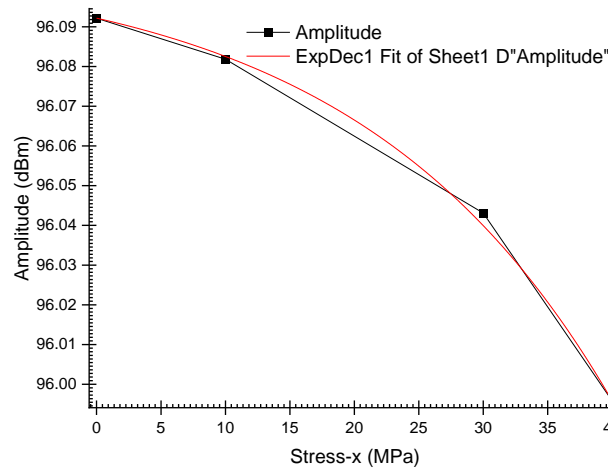


Fig. 11. Final relation between applied stress-x and reflected signal amplitude from the dosimeter.

3. Effect of applied Stress y on dosimeter signal

The stress value, y-component, is included as an external effect of radiation which is changed from 0 to 50 Mpa for region three of the FBG system. Results are shown in Fig. 12 (individual measurements) and 13 for WDM overall measurement.

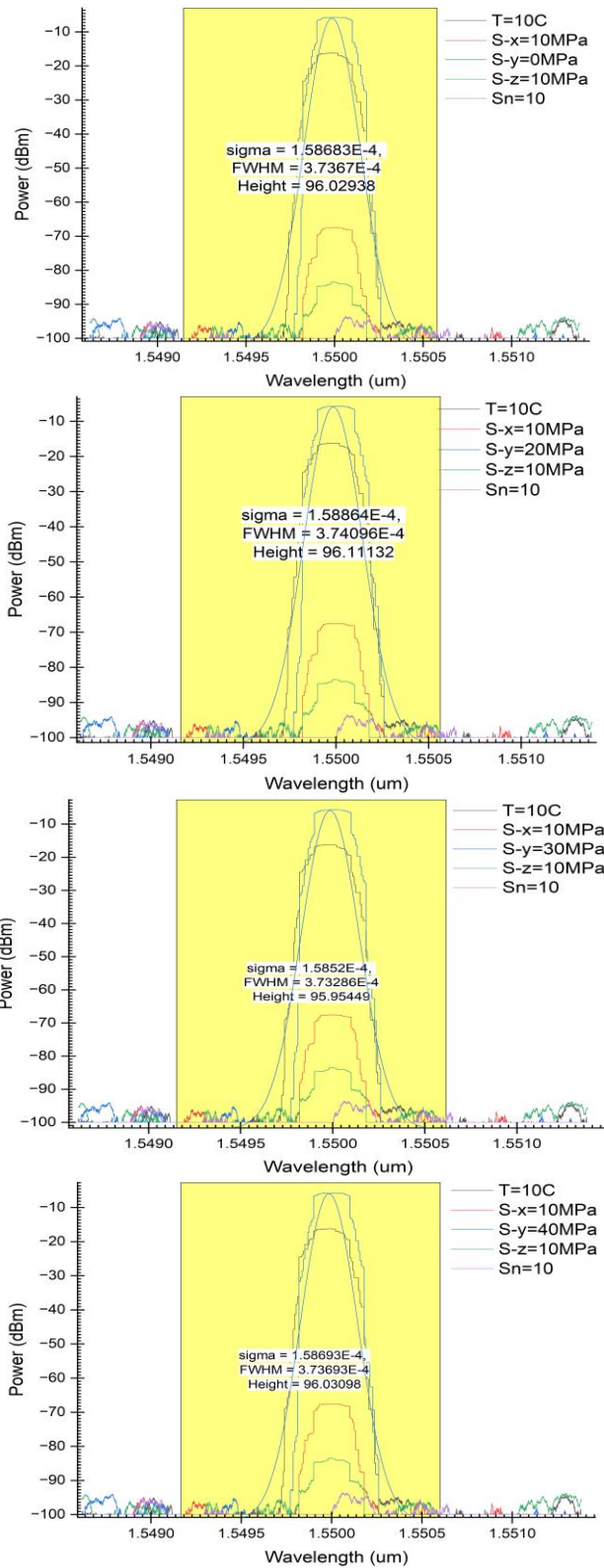


Fig. 12. Individual response for FBG dosimeter regions for stress and strain with applied stress y .

Parameters are given inside each shape.

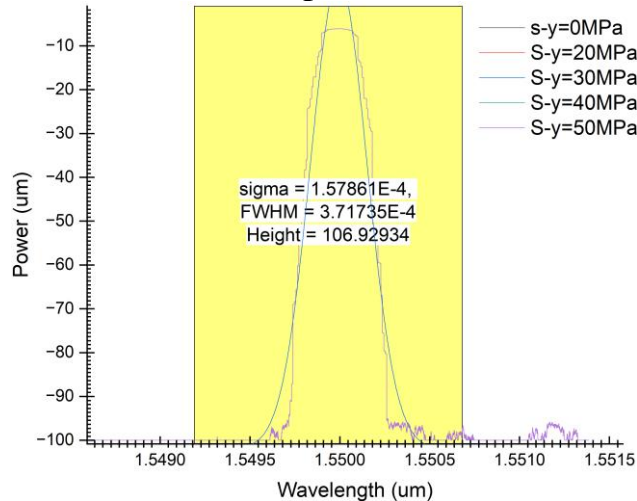


Fig. 13. Multiplexed input WDM for all individual FBG regions reflected signals as a dosimeter response for stress- y variation from 0 to 50MPa.

Statistics for relations between applied stress- y and FWHM and amplitude for the reflected signal from the FBG dosimeter are given in Figs. 14 and 15, respectively. In which the relation in both Figs. are satisfies the square sine relation with applied stress y under the menu of waveform in origin software.

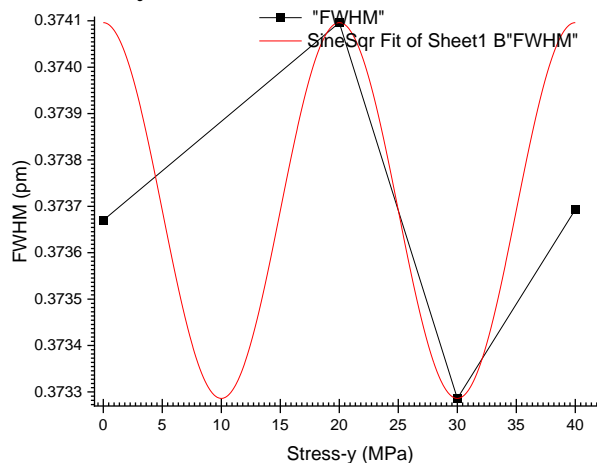


Fig. 14. Final relation between applied stress- y and reflected signal FWHM from the dosimeter.

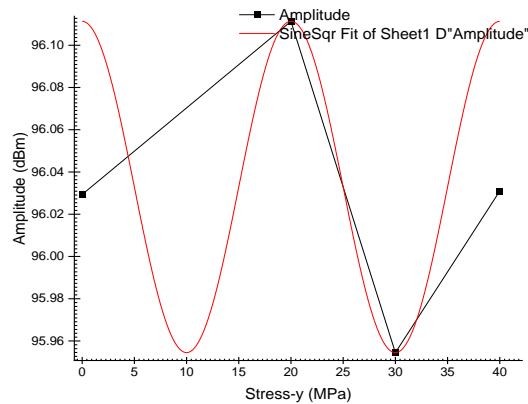
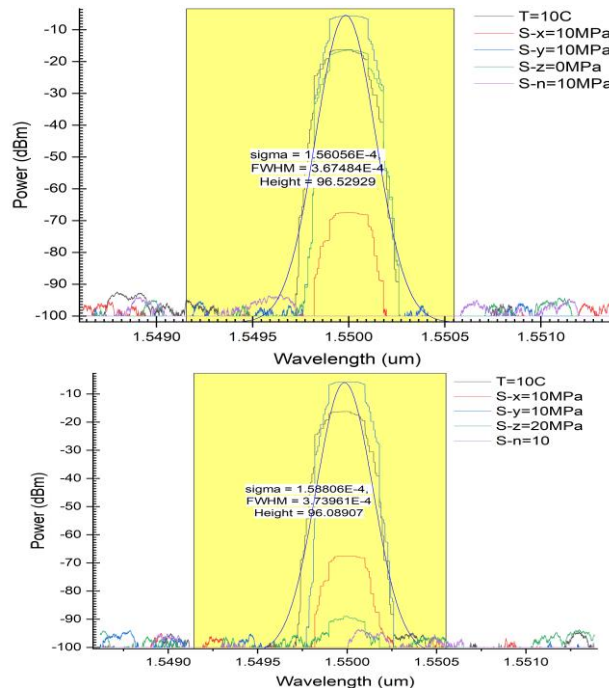


Fig. 15. Final relation between applied stress-y and reflected signal amplitude from the dosimeter.

4. Effect of applied Stress z on dosimeter signal

The stress value, z-component, is included as an external effect of radiation which is changed from 0 to 50 MPa for region four of the FBG system. Results are shown in Fig. 16 (individual measurements) and 17 for WDM overall measurement. It is noticed that FWHM value is changed according to "ExpoDecay3" function with increased stress while amplitude is changed according to inverse for that function, both are shown in Figs. 18 and 19, respectively.



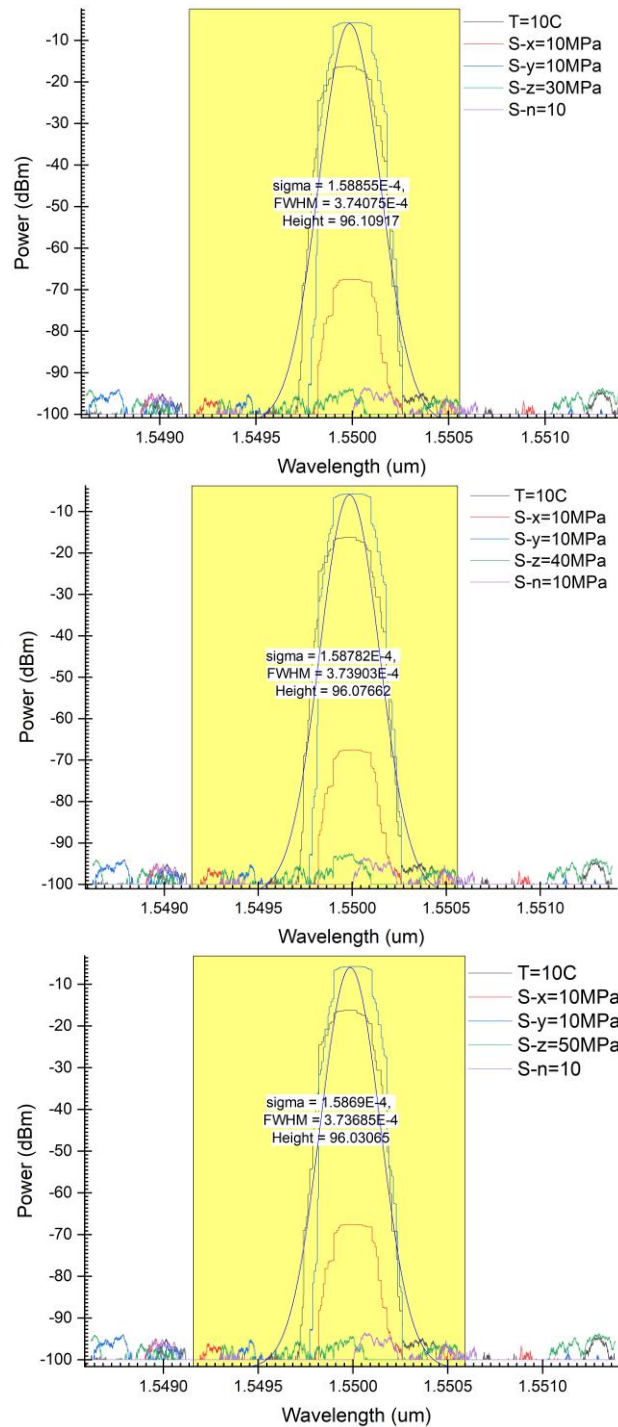


Fig. 16. Individual response for FBG dosimeter regions for stress and strain with applied stress z. Parameters are given inside each shape.

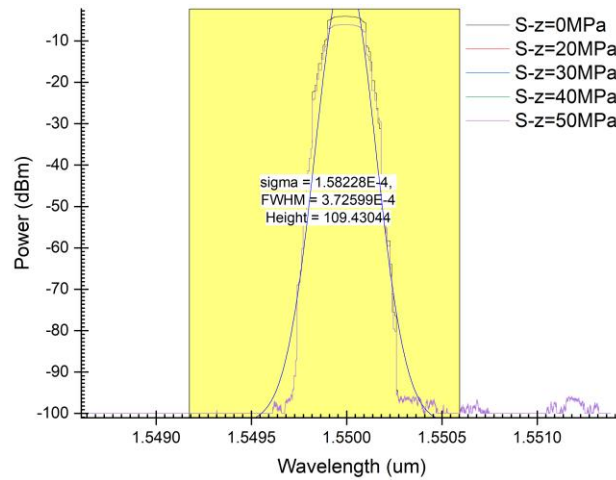


Fig. 17. Multiplexed input WDM for all individual FBG regions reflected signals as a response for stress-z variation from 0 to 50MPa.

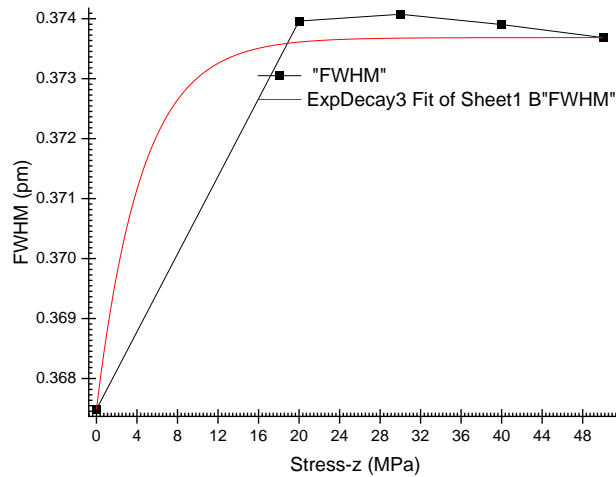


Fig. 18. Final relation between applied stress-z and reflected signal FWHM from the dosimeter.

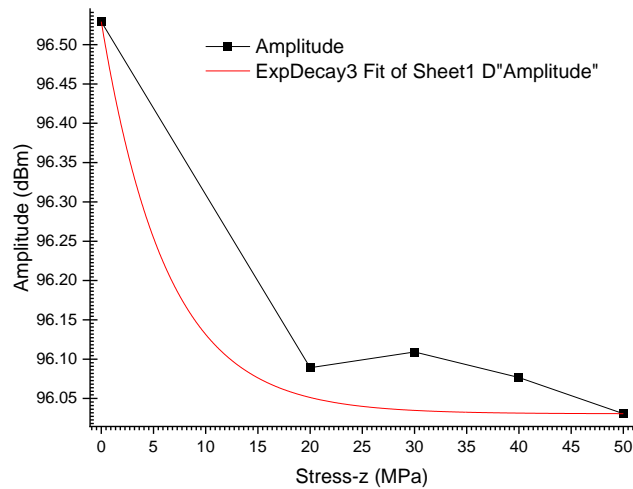
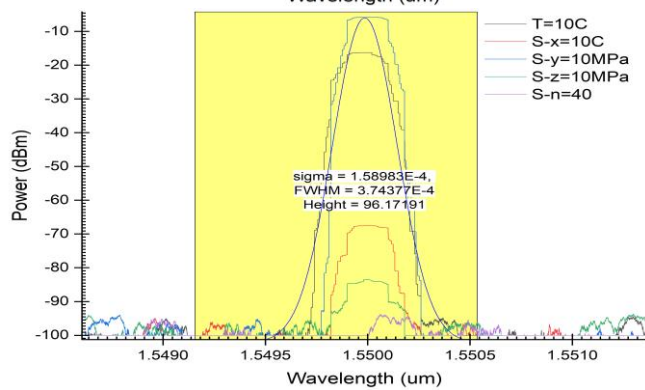
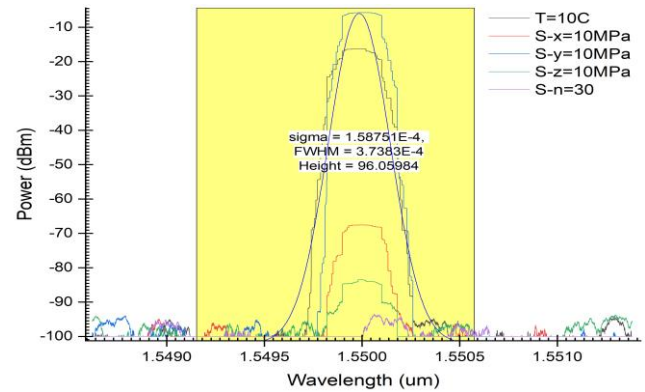
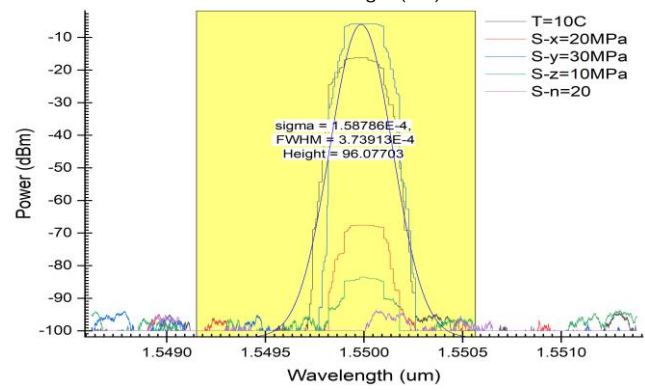
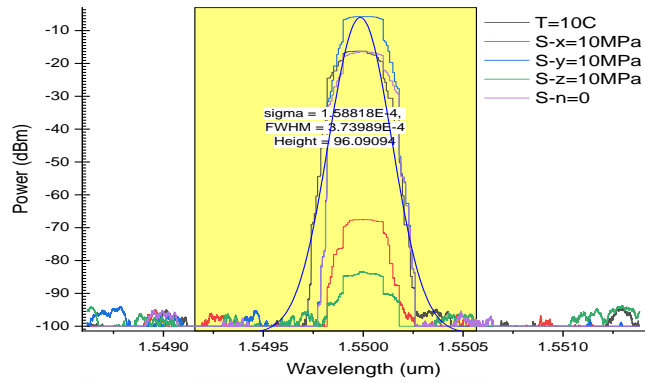


Fig. 19. Final relation between applied stress-z and reflected signal amplitude from the dosimeter.

5. Effect of applied Strain on dosimeter signal

The strain value is also included as an external effect of radiation which is changed from 0 to 50 for region five of the FBG system. Results are shown in Fig. 20 (individual measurements) and 21 for WDM overall measurement. It is noticed that FWHM value is changed according to "Gauss Amplitude" function with increased stress while amplitude is also changed according to it, both are shown in Figs. 21 and 22, respectively.



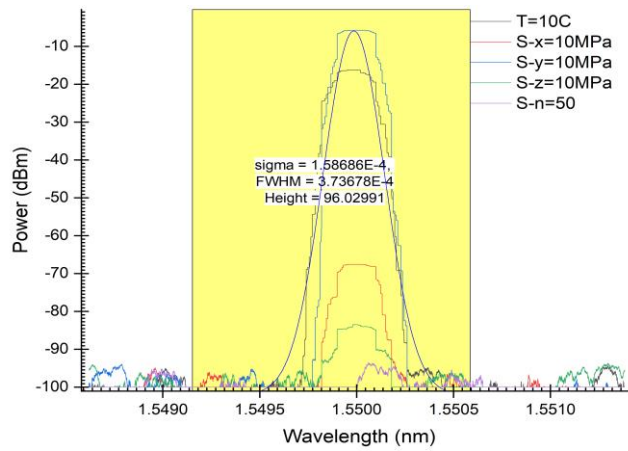


Fig. 20. Individual response for FBG dosimeter regions for stress and strain with applied strain. Parameters are given inside each shape.

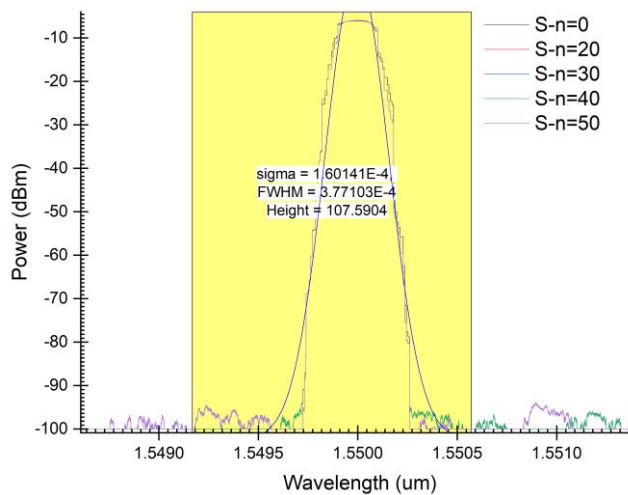


Fig. 21. Multiplexed input WDM for all individual FBG regions reflected signals as a response for strain variation from 0 to 50.

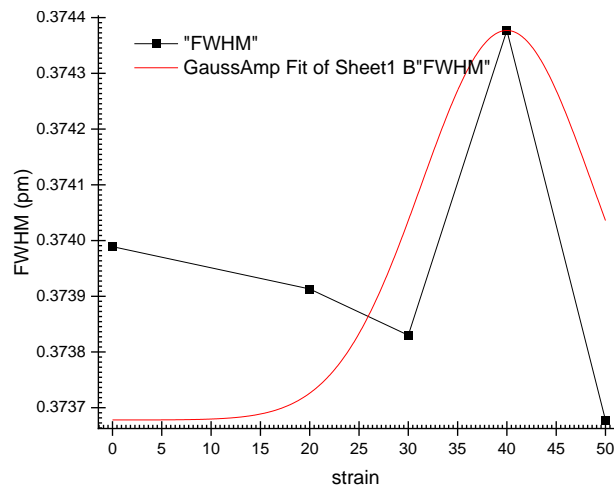


Fig. 21. Final relation between applied strain and reflected signal FWHM from the dosimeter.

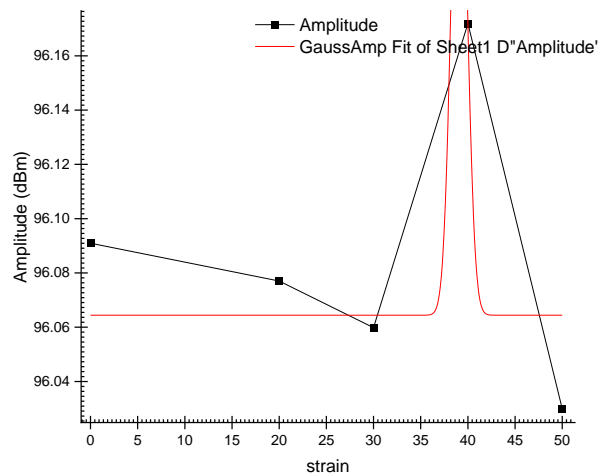


Fig. 22. Final relation between applied strain and reflected signal amplitude from the dosimeter.

The study's surprising findings prompted us to postulate that the FBG structure's effect was the source of the detected signal. It was therefore decided to carry out additional measurements by putting several FBG regions with various thermal qualities to the test. We observed varying dosage FWHM and amplitude responses when we adjusted the FBG dosimeter's areas, which implies that the FBG's structure is where the radiation reaction originates. Thus, it's possible that our dosimeter is functioning as a calibrated calorimeter. The FBG sensor measures the thermal dilatation that occurs in the FBG zones as a result of radio-induced temperature increases upon irradiation ratios. Therefore, the temperature increase caused by the dose

deposition in each FBG zone would be indirectly measured by the FBG-based sensor. The gold standard for radiation dosimetry is calorimetry dosimetry; however, it usually requires a large installation and is not readily applicable in a clinical setting. In a clinical setting, it is usually used to calibrate other equipment that are simpler to use. Although there have been numerous attempts to provide calorimetry in a therapeutic setting, multipoint calorimeters are unheard of.

Ref. [32] mentioned that the dosimetric quantity Q and the dosimeter reading M should ideally be linearly proportionate. However, non-linearity develops after a specific dose range. The kind of dosimeter and its physical attributes determine the linearity range and non-linearity behavior. In the current experiment, many results are nonlinear, which indicates the possibility of overcoming saturation effects arising in conventional dosimeters. Saturation effects destroy dosimeter reading with higher applied doses, which makes it unclear to consider. This is under the effect of FBG division in comparison with standard bulk FBG type.

The integrated response of a dosimetry system is measured by integrating systems. The measured dosimetric quantity for these systems ought to be independent of its rate. A dosimetry system's response, M/Q , should ideally remain constant at two distinct dose rates: D_1 and D_2 . In actuality, the dosage rate may affect the dosimeter results; therefore, the necessary corrections, such as recombination corrections for ionization chambers in pulsed beams, must be made. This correction calculations is absent in case of sensor division due to ignorable saturation value.

III. Conclusions

Division for the FBG sensor dosimeter gives rise to unsaturation for detected radiation doses. Observation of the dynamics of electromagnetic radiation associated with dosimeters indicated more stable signals. Responses for each region integrate those resulting from the neighbor's region. As a result, the observed signal is classified as being more stable than those in bulk FBG dosimeters. Measured response resolution against FWHM and amplitude for each region follow different functions in comparison to the overall function type. This gives a detailed manner of sensing that cannot be observed when including only the overall behavior of the bulk sensor. The FWHM response for the sensor regions to the selected effect is proportional to Sin, ExpDecay, Gauss, SquarSin, ExpDecay3, and GaussAmpl for effects: temperature, x , y , z , and strain, respectively. This observation depends on the

effect type, the range of the selected effect, and its contribution to the photo elastic parameters of the fiber.

Acknowledgments. The authors would like to thank Mustansiriyah University, (www.uomustansiriyah.edu.iq) Baghdad – Iraq for their support in the present work.

References

- [1] A. E.-N. A. Mohamed, A. N. Z. Rashed, M. M. Zaky, A. I. Elsaket and M. A. Gaheen, "Simulative Study of Wavelength Division Multiplexing Fiber Bragg Grating in Nuclear Reactors Monitoring," *Menoufia J. of Electronic Engineering Research (MJEER)*, vol. 28, no. 2, pp. 1-16, 2019.
- [2] A. F. Fernandez, B. Brichard, F. Berghmans, H. E. Rabii, M. Fokine and M. Popov, "Chemical Composition Fiber Gratings in a High Mixed Gamma Neutron Radiation Field," *IEEE transactions on nuclear science*, vol. 53, no. 3, 2006.
- [3] A. Triana, D. Pastor and M. Varón, "Enhancing the Multiplexing Capabilities of Sensing Networks using Spectrally Encoded Fiber Bragg Grating Sensors," *Journal of Lightwave Technology*, vol. 34, no. 19, pp. 4466-4472, 2016.
- [4] R. YJ, "FiberBragg grating sensors: principles and applications. In: Grattan, K.T.V., Meggitt, B.T. (eds) Optical Fiber Sensor Technology," in *Optoelectronics, Imaging and Sensing, vol 2*, Boston, MA, Springer, 1998, p. 355.
- [5] Y. Chamorovskiy, O. V. Butov, A. O. Kolosovskiy, S. M. Popov, V. V. Voloshin, I. L. Vorob'ev and M. Y. Vyatkin, "Metal-coated Bragg grating reflecting fibre," *Optical Fiber Technology*, vol. 34, pp. 30-35, 2017.
- [6] S. Avino, V. D'Avino, A. Giorgini, R. Pacelli, R. Liuzzi, L. Cella, G. Gagliardi and P. D. Natale, "Radiation dosimetry with fiber Bragg gratings," in *Proceedings Volume 9157, 23rd International Conference*

- on *Optical Fibre Sensors*, Santander, Spain, 2014.
- [7] W. A. Jabbar, A. Hemed, M. Fadhala and I. Al-Baidhany, "Effect of GeO₂ Dopants in FBG Sensor Performance for Temperature and Strain," *East European Journal of Physics*, no. 3, pp. 501-508, 2023.
- [8] W. A. Jabbar, A. Hemed, M. Fadhala and I. Al-Baidhany, "Characterization Study of Double Filtered Sensor Length Effect on Strain Sensitivity," *East European Journal of Physics*, no. 3, pp. 509-515, 2023.
- [9] S. M. Khorsheed, A. A. Hemed and M. M. Fdhala, "Investigation of Performance for a Two Regions Superstructure Fiber Bragg Grating," *World Scientific News*, vol. 137, pp. 42-57, 2019.
- [10] E. M. Dianov and V. M. Mashinsky, "Germania-Based Core Optical Fibers," *Journal of Lightwave Technology*, vol. 23, no. 11, pp. 3500-3508, 2005.
- [11] A. Morana, E. Marin, L. Lablonde, T. Blanchet, T. Robin, G. Cheymol, G. Laffont, A. Boukenter, Y. Ouerdane and S. Girard, "Radiation Effects on Fiber Bragg Gratings: Vulnerability and Hardening Studies," *Sensors (Basel)*, vol. 21, no. 22, p. 8175, 2022.
- [12] A. Hemed, M. M. Fdhala and S. M. Khorsheed, "Modified superstructure fiber Bragg grating for a filter application," *Kuwait Journal of Science*, vol. 49, no. 1, pp. 1-18, 2022.
- [13] A. A. Hemed and Z. R. Ghayib, "Effect of Partial Optically Filtered Optoelectronic Feedback on Laser Diode Chaotic Emission," in *2022 4th International Conference on Current Research in Engineering and Science Applications (ICCRESA)*, Baghdad, Iraq., 2023, pp. 165-171.
- [14] A. A. Hemed and Z. R. Gaiab, "Chaotic Dynamics for VCSEL Subjected to Time Delayed and Filtered Injection Using FBG Array Sensor," in *2022 International Conference on Computer Science and Software Engineering (CSASE)*, Duhok, Iraq, 2022, pp. 194-200.

- [15] F. Berghmans, B. Brichard, A. F. Fernandez, A. Gusarov, M. V. Uffelen and S. Girard, "An Introduction to Radiation Effects on Optical Components and Fiber Optic Sensors. Wojtek J. Bock; Israel Gannot; Stoyan Tanev (eds)," in *NATO Science for Peace and Security Series. Springer*, Dordrecht, 2008.
- [16] S. Rizzolo, A. Boukenter, E. Marin, T. Robin, M. Cannas, A. Morana, J. Périssé, J.-R. Macé, Y. Ouerdane, Y. Ouerdane, P. Paillet, C. Marcandella, M. Gaillardin and S. Girard, "Evaluation of Distributed OFDR-Based Sensing Performance in Mixed Neutron/Gamma Radiation Environments," *IEEE Transactions on Nuclear Science*, vol. 64, no. 11, pp. 61-67, 2017.
- [17] D. Baccini, The effect of gamma radiation on fibre Bragg grating sensors, Joondalup, Australia: Edith Cowan University , 2013.
- [18] G. L. Vecchi, Potential of radiation sensitive silica-based optical fibers for dosimetry and regeneration techniques, Saint-Étienne, France: Université Jean Monnet - Saint-Etienne, 2023.
- [19] A. Fernandez, B. Brichard, F. Berghmans and M. Decreton, "Dose rate dependencies in gamma-irradiated fiber Bragg grating filters," *IEEE Transactions on Nuclear Science*, vol. 49, no. 6, pp. 2874-2878, 2002.
- [20] R. Kashyap, Fibre Bragg Gratings, Second Edition, Burlington, MA., USA : Academic Press, 2010.
- [21] R. J. Fielder, R. G. Duncan and M. L. Palmer, "Recent Advancements in Harsh Environment Fiber Optic Sensors: An Enabling Technology of Emerging Nuclear Power Application," *IAEA Meeting*, Knoxville , June 27-28, 2005. .
- [22] J. Troska, J. Batten, K. Gill and F. Vasey, "Radaiton effects in commercial off the shelf single mode optical fibres," in *San Diego, SPIE proceedings*, San Diego, Photonics for Space Environments VI Vol. 3440, pp.112-129, July, 1998 .

- [23] S. A. Slattery, D. N. Nikogosyan and G. Brambilla, "Fiber Bragg grating inscription by high intensity femtosecond UV laser light: comparison with other existing methods of fabrication," *J. Opt. Soc. Am. B*, vol. 22, no. 2, pp. 354-361, 2005.
- [24] G. Yang, S. Lin, J. Jin and N. Song, "Effect of gamma radiation on the reflectance spectrum of fiber Bragg gratings," *Optik*, vol. 124, no. 15, pp. 2246-2250, 2013.
- [25] C. Cuadrado-Labord, Current Trends in Short- and Long-period Fiber Gratings, IntechOpen, 2013.
- [26] K. Krebber, H. Henschel and U. Weinand, "Fibre Bragg gratings as high radiation sensors," *Measurement science and technology*, vol. 17, pp. 1095-1102, 2006.
- [27] A. F. Fernandez, A. Gusarov, F. Berghmans, M. Decretton, P. Megret, M. Blondel and A. Delchambre, "Long term irradiation of fibre Bragg gratings in a low dose rate gamma neutron radiation field," *SPIE*, vol. 4823, pp. 205-212, 2002.
- [28] S. Lin, N. Song, J. Jin, X. Wang and G. Yang, "Effect of Grating Fabrication on Radiation Sensitivity of Fibre Bragg Gratings in Gamma Radiation Field," *IEEE Transactions on Nuclear Science*, vol. 58, no. 4, pp. 2111-2117, 2011.
- [29] H. Henschel, S. K. Hoeffgen, K. Krebber, J. Kuhnenn and U. Weinand, "Influence of Fiber Composition and Grating Fabrication on the Radiation Sensitivity of Fiber Bragg Gratings," *IEEE Transactions on Nuclear Science*, vol. 55, no. 4, pp. 2235-2242, 2008.
- [30] S. Lin, N. Song, J. Jin, X. Wang and G. Yang, "Effect of Grating Fabrication on Radiation Sensitivity of Fibre Bragg Gratings in Gamma Radiation Field," *IEEE Transactions on Nuclear Science*, vol. 58, no. 4, pp. 2111-2117, 2011.
- [31] A. Morana, E. Marin, L. Lablonde, T. Blanchet, T. Robin, G. Cheymol,

G. Laffont, A. Boukenter, Y. Ouerdane and S. Girard, "Radiation Effects on Fiber Bragg Gratings: Vulnerability and Hardening Studies," *Sensors (Basel)*, vol. 22(21), p. 8175, 2022.

[32] R. I, "Radiation Dosimeters," *British journal of cancer*, vol. 98, no. 1020, 2008.

تأثير تجزئة مقياس الجرعة لفايبر براغ على قابلية التحسس للجرع الاشعاعية المنخفضة
تغريد خالد حميد

taghreedkhalid@uomustansiriyah.edu.iq

وسماء عبدالستار جبار

wasmaajabbar@uomustansiriyah.edu.iq

زينتة محمود شعبان الداغستاني

kkzlls1234@gmail.com

ايسر عبدالحسين حمد

ayser.hemed@uomustansiriyah.edu.iq

سامي سلمان جيايد

dr.sami@uomustansiriyah.edu.iq

قسم الفيزياء، كلية التربية، الجامعة المستنصرية، بغداد-العراق

مستخلص البحث:

في الدراسة الافتراضية الحالية القائمة على برنامج Optisystem 21، تم تطوير متحسس فايبر براغ لقياس الجرعة الواطنة بطريقة تجزئة الى خمس مناطق. تمتلك كل المناطق نفس الخصائص البصرية لمادة الليف الضوئي المستخدم وهي ثنائي أكسيد السليكا SiO_2 . كما متعارف في مجال متحسسات الاشعاع فانه يتم ادخال مواد مطعمة بنسب محدد لغرض زيادة قابلية التحسس لثنائي اوكسيد السليكا. التصميم الجديد يستغني عن استخدام هذه الشوائب التطعيمية وهو قابل للاستشعار بدونها. توصلت النتائج المتحصلة الى الحصول على نسب تحسس متزايدة باستخدام تقنية التجزئة مقارنة باستخدام كتلة واحدة مدمجة من الليف الضوئي. قياسات التحسس اعتمدت على حساب دالة الاستعراض FWHM وكذلك قياس سعة الإشارة المرصودة من الجزء الحائد عن ليف براغ الخاضع للإشعاع. تم حساب كلا من الدالتين السابقتين بشكل منفرد كدالة للمؤثرات المعتمدة كتداعيات للخضوع للإشعاع وهي: الحرارة، اجهاد مركبة x، اجهاد مركبة y، اجهاد مركبة z، الانفعال. من خلال العلاقات الناتجة بين كل مؤثر وما يقابله من استعراض وسعة تم اختيار دوال معايرة قياسية من برنامج Origin. اكدت النتائج المتحصلة على فعالية التجزئة على هذا النوع من القياسات كتأثيرات جانبية لإشعاع x وكذلك اشعاع y.

الكلمات المفتاحية: مقياس الجرعات، محرز اليف براك، الاشعة السينية، اشعة كاما، دالة عرض الخط، الحيود.

ملاحظة: هل البحث مستل من رسالة ماجستير او اطروحة دكتوراه ؟ كلا